Subhankar Dolai,[1] Li Xie,[1] Dan Zhu,[1] Tao Liang,[1] Tairan Qin,[1] Huanli Xie,[1] Youhou Kang,[1] Edwin R. Chapman,[2] and Herbert Y. Gaisano[1,3]

Synaptotagmin-7 Functions to Replenish Insulin Granules for Exocytosis in Human Islet β-Cells

Diabetes 2016;65:1962–1976 | DOI: 10.2337/db15-1436

Synaptotagmin (Syt)-7, a major component of the exocytotic machinery in neurons, is also the major Syt in rodent pancreatic β-cells shown to mediate glucose-stimulated insulin secretion (GSIS). However, Syt-7's precise exocytotic actions in β-cells remain unknown. We show that Syt-7 is abundant in human β-cells. Adenovirus–short hairpin RNA knockdown (KD) of Syt-7 in human islets reduced first- and second-phase GSIS attributed to the reduction of exocytosis of predocked and newcomer insulin secretory granules (SGs). Glucose stimulation expectedly induced Syt-7 association in a Ca^{2+}-dependent manner with syntaxin-3 and syntaxin-1A soluble N-ethylmaleimide–sensitive factor attachment protein receptor (SNARE) complexes known to mediate exocytosis of newcomer and predocked SGs, respectively. However, Syt-7-KD did not disrupt SNARE complex assembly. Instead, electron microscopy analysis showed that Syt-7-KD reduced the recruitment of SGs to the plasma membrane after glucose-stimulated depletion, which could not be rescued by glucagon-like peptide 1 pretreatment. To assess the possibility that this new action of Syt-7 on SG recruitment may involve calmodulin (CaM), pretreatment of islets with CaM blocker calmidazolium showed effects very similar to those of Syt-7-KD. Syt-7 therefore plays a novel more dominant function in the replenishment of releasable SG pools in human β-cells than its previously purported role in exocytotic fusion per se.

In exocytosis, soluble N-ethylmaleimide–sensitive factor attachment protein receptor (SNARE) proteins on secretory granules (SGs) and plasma membrane (PM) are assembled into a complex assisted by accessory proteins to hold SGs close to the PM (1). Synaptotagmins (Syts) are major Ca^{2+} sensor proteins attached to SNARE complexes, which, when bound to Ca^{2+}, trigger SNARE complex–mediated exocytotic fusion (1–3). In pancreatic islet β-cells, recruitment and exocytosis of insulin SGs exhibit a biphasic glucose-stimulated insulin secretory (GSIS) pattern consisting of a robust first phase followed by a sustained second phase (4). Insulin SGs undergo several modes of exocytosis that underlie each of the two phases of GSIS. In the first mode, SGs are recruited to dock on the PM followed by priming; then these SGs sit on the PM for an indefinite time (hence being termed "predocked" SGs) until Ca^{2+}-triggered exocytosis. Predocked SGs are purported to form the readily releasable pool (RRP) that is a major contributor to first-phase GSIS (5). In the second mode, insulin SGs are mobilized from a reserve pool (RP) in the β-cell interior to the PM to undergo fusion with only a short period or almost no docking time at the PM. These SGs, coined "newcomer" SGs, are responsible for almost all of second-phase GSIS and a substantial proportion of first-phase GSIS (6–11). First-phase release of predocked SGs requires high intracellular calcium concentration (half-maximal effective concentration value of 10 μmol/L) (12,13), whereas second-phase secretion is operated under lower intracellular calcium concentration, the latter indicating a different pool of SGs (newcomer SGs) that exhibit very high Ca^{2+} affinity (half-maximal effective concentration value of a few micromoles) (14). Taken together, these reports suggest the involvement of different SNARE complexes and cognate Ca^{2+} sensors for predocked and newcomer SGs (7). We determined the SNARE fusion machinery

[1]Department of Medicine, University of Toronto, Toronto, ON, Canada
[2]Department of Neuroscience, Howard Hughes Medical Institute, University of Wisconsin-Madison, Madison, WI
[3]Department of Physiology, University of Toronto, Toronto, ON, Canada
Corresponding author: Herbert Y. Gaisano, herbert.gaisano@utoronto.ca.

Received 19 October 2015 and accepted 16 April 2016.

This article contains Supplementary Data online at http://diabetes.diabetesjournals.org/lookup/suppl/doi:10.2337/db15-1436/-/DC1.

of newcomer SGs, which consists of Syn-3, VAMP8, and accessory priming factor Munc18b (15–17). This is distinct from the fusion machinery of predocked SGs (i.e., Syn-1A, VAMP2, and Munc18a) (5–7). However, what the putative Ca^{2+} sensor(s) is for predocked and newcomer SGs has not been definitively demonstrated.

Syts constitute a family of transmembrane proteins with two cytoplasmic C2 domains (C2A and C2B) that exhibit distinct binding properties to effectors Ca^{2+}, SNARE proteins, and phospholipids (2,3). Of 17 mammalian Syt isoforms, several have been postulated to regulate insulin SG exocytosis (18), of which Syt-7 appears to be the putative one (19–22). This was definitively shown by genetic deletion of Syt-7 in mice, which reduced biphasic GSIS (21,22). However, in those studies (21,22), the precise role of Syt-7 in insulin SG exocytosis per se was not elucidated. It was assumed that Syt-7's major action is to drive *t*-SNAREs (Syn-1A and SNAP25) to completion of SNARE complex assembly leading to fusion (2). Unexpectedly, in the current study, we used human islet β-cells to demonstrate that the more dominant role of Syt-7 is to recruit insulin SGs from the cell interior to replenish releasable SG pools after their depletion from stimulation. These multimodal actions of Syt-7 can potentially compensate for the defective exocytosis in type 2 diabetic β-cells (5,23,24).

RESEARCH DESIGN AND METHODS

Islets and Insulin Secretion Assay

Human islets were from Institutional Review Board–approved 15 nondiabetic healthy donors (7 males/8 females; age: 55.47 ± 14.35 years; BMI: 27.79 ± 4.39; HbA_{1c}: 5.63 ± 0.36% [38.27 ± 3.95 mmol/mol]) isolated and provided by IsletCore (P. Macdonald, University of Alberta, Alberta, Canada), and use was approved by the Institutional Review Board at University of Toronto. Isolation and culture of islets and INS-1 cells (832/13; C. Newgard, Duke University, Durham, NC), adenoviral transduction, and insulin secretion were performed as previously described (17,25). Islets from Sprague-Dawley male rats (275–300 g) were isolated by collagenase digestion. Islets were dispersed into single β-cells with Ca^{2+}/Mg^{2+}-free PBS containing 5 mmol/L EDTA and 0.25 mg/mL trypsin. Islets, β-cells, and INS-1, cultured in supplemented RPMI 1640 (Gibco) medium, were transduced with 10^{10} plaque-forming units/mL red fluorescence protein (RFP)–tagged Syt-7 targeting short hairpin RNA (shRNA) adenovirus (Ad-Syt-7-shRNA/RFP; shRNA sequence indicated in the text) or RFP-tagged nontargeting scrambled shRNA adenovirus (Ad-*sc*-shRNA/RFP) as control, both from Vector Biolabs (Philadelphia, PA). Cells intended for total internal reflection fluorescence microscopy (TIRFM) were coinfected with adenovirus encoding neuropeptide Y-enhanced green fluorescent protein (NPY-EGFP). For perifusion, 48-h posttransduced islets (50 islets) were loaded in perfusion chambers (~1.3 mL capacity) and perifused with Krebs-Ringer bicarbonate (KRB) buffer at a flow rate of ~1 mL/min (37°C). Stimulation was with 2.8 or 16.7 mmol/L glucose. Secreted insulin was measured by radioimmunoassay (Linco Research, St. Louis, MO). Static GSIS on INS-1 cells was assessed using a homogenous time-resolved fluorescence insulin assay kit (Cisbio, Bedford, MA) on a PHERAstar plate reader (BMG Labtech, Ortenberg, Germany) (26). Levels of secreted insulin from islets and INS-1 were normalized to total insulin content.

Binding Assays, Western Blotting, and Antibody Specificity

Recombinant GST fusion proteins, GST pulldown, and immunoprecipitation (IP) assays were performed as we previously reported (27). For generation of GST proteins, pGEX plasmids with cytoplasmic domains of Syt-7 including C2A (residues 134–263 GST-C2A), C2B (residues 243–403, GST-C2B), C2AB (residues 134–403, GST-C2AB), and quadruple Ca^{2+}-binding mutant 4D/N (D225,227,357,359N; GST-C2AB4D/N) were transformed into *Escherichia coli* BL21 (DE3) for protein expression. GST-fusion proteins were then purified using glutathione-Sepharose beads. HEK293 cells were transfected with pcDNA3.1-Syn-1A or pcDNA3.1-Syn-3 plasmids using Lipofectamine 2000 (Invitrogen); 48-h posttransfected cells were then washed with PBS and lysed in binding buffer (20 mmol/L HEPES, 100 mmol/L KCl, 1.5% Triton X-100, 1 μg/ml leupeptin, and 10 μg/ml aprotinin [pH 7.4]) at 4°C. For Ca^{2+} dependence studies, lysis buffer (containing 10 μmol/L $CaCl_2$) was supplemented with 2 mmol/L EGTA. Lysates were clarified (21,000*g*, 30 min, 4°C) and 400 μg of soluble supernatant mixed with 200 pmol of glutathione-agarose beads bound to GST-C2AB, GST-C2AB4D/N, GST-C2A, GST-C2B, or GST (as negative control), at 4°C with constant agitation for 2 h.

For IP, 70–75% confluent INS-1 cells were transduced with Ad-Syt-7-shRNA/RFP versus control Ad-*sc*-shRNA/RFP; 48-h posttransduced cells were then washed with PBS and incubated with Krebs-Ringer HEPES buffer (30 min, 37°C) at 0.8 mmol/L glucose to obtain uniform basal condition and then further incubated with 10 nmol/L glucagon-like peptide 1 (GLP-1) (30 min), followed by stimulation with 16.7 mmol/L glucose (containing 10 nmol/L GLP-1) for 30 min; control basal condition is sustained 0.8 mmol/L glucose treatment. Treated cells were harvested and lysed by sonication in lysis buffer (25 mmol/L HEPES, 100 mmol/L KCl, 1.5% Triton X-100, and protease inhibitors). A total of 500 μg protein extract from each condition was precleared with 50 μL of protein A-agarose beads (Molecular Probes, Eugene, OR) and then subjected to IP with specific 1.2 to 2.0 μg Syn-1A or Syn-3 antibodies linked to protein A-agarose beads. Beads obtained from GST pulled down or IP were washed three times with lysis/binding buffers, and bound proteins were then eluted by boiling in SDS sample buffer, separated on 12–15% SDS-PAGE, and identified by specific primary antibodies.

Syt-7 antibody (catalog no. 105173; SySy, Goettingen, Germany) specificity for human islet Syt-7 isoforms is shown in Supplementary Fig. 1. All other antibodies used were commercial antibodies (Synaptic System, Goettingen, Germany), except for VAMP2 (gift from Anson Lowe, Stanford University, Stanford, CA) and Munc18b (gift from V. Olkkonen, Minerva Foundation Institute for Medical Research, Helsinki, Finland); their use we had previously reported (15,17).

Confocal Immunofluorescence Microscopy

Islet and β-cell imaging was performed with a Leica laser scanning confocal microscope system (DMIRE2; Leica Microsystems, Wetzlar, Germany) with ×20 (numerical aperture 0.75) and ×60 (numerical aperture 1.4) oil immersion objectives as previously described (17). Primary antibodies include insulin (guinea pig, 1:200; Dako Diagnostics, Mississauga, Ontario, Canada), glucagon (mouse, 1:200; NovoCastra Laboratories, Leica Microsystems), and somatostatin (rabbit, 1:200; GeneTex Inc., Irvine, CA) and rabbit anti–Syt-7 antibody (1:200; Synaptic System). Deconvolution algorithm was applied to images to remove out-of-focus background noise. Colocalization was quantified using Volocity software (PerkinElmer, Waltham, MA). Regions of interest (ROIs) were outlined; the number of colocalized pixels within a particular ROI was determined and expressed as percentage of total pixels within that ROI.

Electrophysiology

Whole-cell patch clamp recordings (28) were made on RFP-expressing β-cells. Recordings were conducted using a EPC10 amplifier, Pulse and X-chart software programs (HEKA Electronik, Lambrecht, Germany). Intracellular solution contains (in millimoles): 125 cesium glutamate, 10 CsCl, 10 NaCl, 1 $MgCl_2$, 5 HEPES, 0.05 EGTA, 3 MgATP, and 0.1 cAMP (pH 7.2); bath solution contains (in millimoles): 118 NaCl, 5.6 KCl, 1.2 $MgCl_2$, 10 $CaCl_2$, 20 tetraethylammonium chloride, 5 HEPES, and 5 D-glucose (pH 7.4) at 30°C. Exocytic events were elicited by a train of eight 500-ms depolarization pulses (1-Hz stimulation frequency) from −70 to 0 mV. Data were analyzed with Igor Pro software (WaveMetrics, Lake Oswego, OR).

Electron Microscopy

This was performed as we previously described (16,25). Islets were fixed with Karnovsky style fixative (with 3.2% paraformaldehyde, 2.5% glutaraldehyde, and 0.1 mol/L sodium cacodylate buffer with 5 mmol/L $CaCl_2$ [pH 6.5]), postfixed with 1% osmium tetroxide. Samples were preembedded in 1% uranyl acetate, dehydrated, and infiltrated with epon 812 resin polymerization completed with epoxy resin. Ultrathin sectioning (80 nm) was by Reichert Ultracut Emicrotome; samples were collected on 200 mesh copper grids, counterstained with saturated 4% uranyl acetate followed by Reynold's lead citrate, and then examined and photographed in a Hitachi H-7000 transmission electron microscope (Hitachi) at an accelerating voltage of 75 kV, by using an AMT XR-60 camera and AMT software (Advanced Microscopy Techniques). Random images of β-cells were acquired from three different islet isolations (five different grids per experiments) for Control and Syt-7-knockdown (KD) islets at ×5,000 and ×17,000 magnification. For morphometric analysis (ImageJ; National Institutes of Health; http://rsb.info.nih.gov/ij), total cytoplasmic area within 1.5 μm distance from PM and without nucleus was measured after scale adjustment and then the total number of SGs counted within this area. Concentric shells of 0.2 μm from PM to the cell interior up to 1.5 μm from PM were drawn, and then SGs with their granule center within the shell were counted (29) and expressed as percentage of the average density of total cytoplasmic SGs within 1.5 μm from PM.

TIRFM

TIRFM was performed with a Nikon TE2000U inverted microscope (Nikon, Mississauga, Ontario, Canada) using an established prismless and through-the-lens configuration as we previously described (16,17,30). β-Cells expressing both RFP and NPY-EGFP were selected for imaging, and a total of 6,000 frames were acquired at 5 Hz with 100-ms exposure time. Cells, initially bathed for 30 min in KRB buffer containing 2.8 mmol/L glucose, were stimulated by KRB buffer containing 16.7 mmol/L glucose at a flow rate of 1 mL/min. Flashes of fluorescence that exceed by five times the SD of basal fluorescence fluctuation were considered as fusion events and categorized into: *1*) predocked SGs (already visible on the PM without stimulation), *2*) newcomer-no dock SGs (residence time of <200 ms on PM), and *3*) newcomer-short dock (appeared then remaining on PM for >200 ms before fusion occurred). A concentric circle (~5 pixels with a pixel size of 267 nm, corresponding to ~1.335 μm diameter) was used to center on selected SGs to characterize the evolution of fluorescence over time of single SGs on background-subtracted images. Fluorescence of individual SGs was measured as mean brightness of the defined circle. The number of predocked SGs was counted and averaged at the first 2 min prior to stimulation. Mobilization and exocytosis of SGs were analyzed by Matlab (MathWorks, Natick, MA), ImageJ (National Institutes of Health), and Igor Pro software (WaveMetrics, Portland, OR). All recordings were performed at 37°C.

Statistical Analysis

All data are presented as means ± SEM. Statistical significance was assessed by repeated-measures ANOVA or Student *t* test using Origin 6 or Microsoft Excel (Microsoft). Significant difference is indicated by asterisks ($^*P < 0.05$, $^{**}P < 0.01$, $^{***}P < 0.001$).

RESULTS

Syt-7 Is Abundant in Insulin SGs of Human β-Cells and Its Expression Depleted by Adeno-shRNA

Syt-7 was previously detected in rodent β-cells (20,21). Syt-7 expression in human islets (Fig. 1*A*, top) and dispersed insulin-containing β-cells (Fig. 1*A*, bottom, arrows) was shown using Syt-7–specific antibody. Syt-7 is also

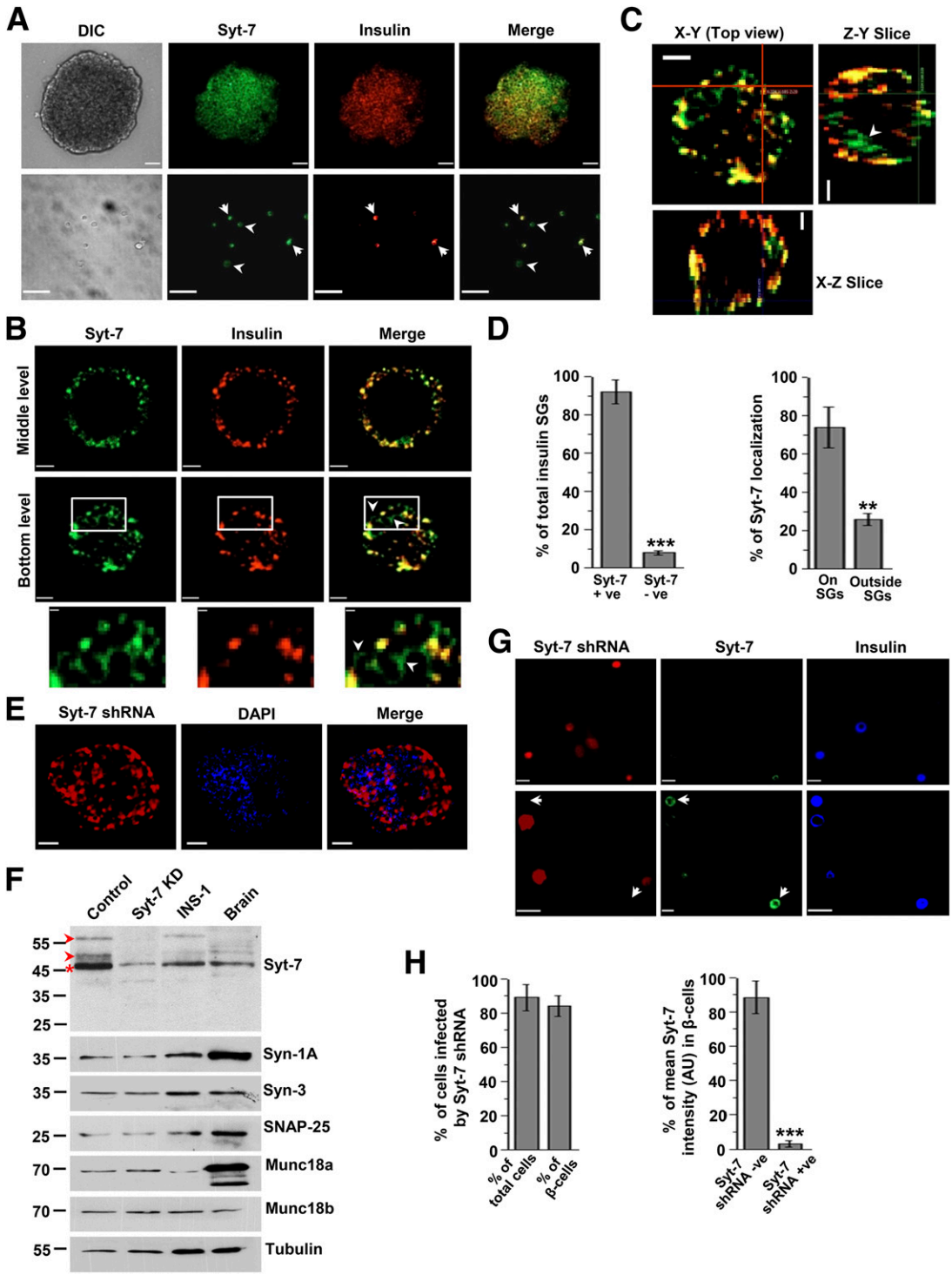

Figure 1—Syt-7 is abundant in insulin SGs of human islet β-cells and its expression is effectively depleted by adeno-shRNA. *A*: Representative immunofluorescence images showed that Syt-7 (green) is present in insulin-containing (red) β-cells in human pancreatic islet (top) and dispersed islet β-cells (arrows, bottom). Differential interference contrast (DIC) images to see all of the cells are shown. Insulin-negative but Syt-7–positive cells were shown to be α- and δ-cells in Supplementary Fig. 1*A*. Scale bars, 50 μm. *B*: Single 0.4-μm–thick optical sections (middle and bottom levels of the cell shown) of a representative single human β-cell show Syt-7 to be largely localized on insulin SGs. Scale bars, 2 μm. Boxed areas are shown enlarged (×4) at the bottom to more clearly show that Syt-7 is present not only in insulin SGs (yellow in merge image) but also in cytoplasmic areas outside insulin SGs (green in merge image, arrowheads). Scale bars, 0.5 μm. The bottom level image is depicted in *C* as cross-sectional views in three dimensions (XY, XZ, and YZ). *D*: Quantification of Syt-7–positive insulin SGs (left) and Syt-7 colocalization with insulin SGs (right) in ≥100 cells. *E*: Representative confocal images of Ad-Syt-7–shRNA/RFP-infected (red) human islets. Individual cells were detected by nuclear stain DAPI (blue), which showed that some islet core cells were not infected; shown better in the merged image. Scale bars, 40 μm. *F*: Immunoblots of human islets (30 μg) subjected to Ad-Syt-7–shRNA/RFP infection (Syt-7-KD) compared with control (Ad-*sc*-shRNA/RFP infection) show efficient KD of Syt-7 isoforms including the dominant 45-kD isoform (indicated by asterisk) and less abundant larger isoforms (indicated by arrowheads). Expression of Syt-7

found in glucagon-containing α-cells (Supplementary Fig. 1*A*, top, arrows) and somatostatin-containing δ-cells (Supplementary Fig. 1*A*, bottom), consistent with previous reports in mouse islets (21,31). In dispersed β-cells, Syt-7 is most abundant on insulin SGs (Fig. 1*B*, yellow in Merge images) with substantial proportions also found outside (green in Merge images) the SGs (Fig. 1*B*, bottom, Fig. 1*C*, arrowheads). Quantification revealed that 92 ± 6.2% of insulin SGs are Syt-7 positive (Fig. 1*D*, left). Nonetheless, although 74 ± 10.6% of Syt-7 is colocalized with insulin SGs (Fig. 1*D*, right), a small but substantial portion of Syt-7 is found in cytoplasmic compartments (indicated by arrowheads in Fig. 1*B*, enlarged at bottom), which might play a role in SG recruitment assessed in the latter part of this study.

The function of endogenous Syt-7 was assessed by Ad-Syt-7–shRNA/RFP (shRNA primers targeting 5′-AGA-CAA-GCG-GGT-AGA-GAA-A-3′, coexpressing RFP, 10^{10} plaque-forming units) KD, which showed efficient transduction of 72 ± 8.7% (RFP-expressing cells in Fig. 1*E*) including islet core cells. Syt-7-KD efficiency in human islets by the virus showed a similar 75% reduction of the abundantly expressed ~45 kDa isoform (indicated by asterisk, Fig. 1*F* and Supplementary Fig. 1*B*) after 48-h infection (optimized with rat islets [Supplementary Fig. 1*C* and *D*]). Other less abundant larger spliced variants of Syt-7 (32) were detected; their expression was also abolished in Syt-7–depleted islets (Fig. 1*F*, arrowheads). Specificity of Syt-7 antibody toward these splice variants was verified with recombinant Syt-7–C2AB preincubated Syt-7 antibody, which reduced staining of ~45 kDa Syt-7 by 84% and other larger splice variants by 64 and 73% (Supplementary Fig. 1*E*). Syt-7 depletion did not alter the expression of Syt-interacting syntaxins Syn-1A and Syn-3, their respective cognate SM (Sec1/Munc18-like) proteins Munc18a and Munc18b, and SNAP25 (Fig. 1*F*; Supplementary Fig. 1*B*). In dispersed islet cells, efficiency of Syt-7-KD is shown by ablation of endogenous Syt-7 in RFP-expressing cells (Fig. 1*G*), with Syt-7 expression (green) intact in a few RFP-negative cells (arrows). In this study, transfection efficiency was 89 ± 7.8% of dispersed cells and 84 ± 6.6% of β-cells (Fig. 1*H*, left) with 96.7% depletion in Syt-7 expression (Fig. 1*H*, right) in the transfected β-cells. This also validates the specificity of our Syt-7 antibody (Fig. 1*G*).

Syt-7 Depletion in Human Islets Reduces Biphasic GSIS by Actions on Releasable SG Pools

Human islet perifusion assays using control (Ad-scrambled [*sc*]-shRNA/RFP–infected) and Syt-7-KD (Ad-Syt-7-shRNA/RFP–infected) human islets showed that 16.7 mmol/L GSIS was reduced by 35.5% in Syt-7-KD islets in first phase (Fig. 2*A*) (area under the curve analysis, Syt-7-KD: 6.37 ± 0.66, control: 9.88 ± 1.05; $P < 0.01$) and by 39.5% in second phase (Syt-7-KD: 7.18 ± 0.81, control: 11.87 ± 2.8; $P = 0.02$), with no difference in basal release (2.8 mmol/L glucose) or total cellular insulin content (control: 1.23 ± 0.05 μg/well; Syt-7-KD: 1.19 ± 0.04 μg/well). These results are similar to the 40% reduction in GSIS reported in Syt-7-knockout mice islets (21). We then assessed for whether GLP-1 could rescue (33) the Syt-7-KD–induced secretory defect. A total of 10 nmol/L GLP-1 potentiated biphasic GSIS was similarly reduced in Syt-7-KD islets with 29% reduction in first phase (Fig. 2*B*) (Syt-7-KD: 10.21 ± 0.59, control: 14.39 ± 0.56; $P < 0.03$) and 36.5% reduction in second phase (Syt-7-KD: 8.12 ± 0.71, control: 12.79 ± 1.26; $P = 0.02$). As we have used INS-1 for the latter protein binding studies, we also assessed for Ad-Syt-7–shRNA/RFP treatment of INS-1 (≥78% KD of Syt-7 protein expression) (Supplementary Fig. 3*C*), which caused a comparable 47.6% reduction in 16.7 mmol/L GSIS (Syt-7-KD: 0.75 ± 0.11, control: 1.43 ± 0.16; $P = 0.02$) and 41% reduction in GLP-1–potentiated GSIS (Syt-7-KD: 1.29 ± 0.09, control: 2.19 ± 0.15; $P = 0.02$), with no effect on basal release (Fig. 2*C*).

Exocytosis of RRP and mobilization of RP in single β-cells is estimated by patch-clamp membrane capacitance (Cm) measurements, purported to correspond to first- and second-phase GSIS from whole islets, respectively (4). Dispersed RFP-expressing β-cells (transfected with Ad-*sc*-shRNA/RFP or Ad-Syt-7–shRNA/RFP) were stimulated by a train of 10 depolarization pulses, in which the first two pulses approximate the size of the RRP of primed fusion-ready SGs and subsequent pulses estimate the rate of SG refilling or mobilization from RPs to the RRP, where SGs are subsequently primed for fusion competence. Syt-7–shRNA/RFP-expressing cells are likely to be completely depleted of Syt-7 (Fig. 1*G* and *H*). β-Cells were identified by the larger cell size (averaging 10 pF) (34). Cm increases in Syt-7-KD β-cells were greatly inhibited at every depolarizing pulse (Fig. 2*D*, left and middle) compared with control cells. The size of RRP ($\Delta Cm_{1st\text{-}2nd}$ pulse) was reduced by 60% (Syt-7-KD: 4.57 ± 1.28 fF/pF; control: 11.5 ± 2.14 fF/pF; $P < 0.05$) (Fig. 2*D*, right) and rate of SG refilling/mobilization ($\Delta Cm_{3rd\text{-}10th}$ pulse) reduced by 49% (Syt-7-KD: 9.48 ± 2.79 fF/pF; control: 18.72 ± 3.02 fF/pF; $P < 0.05$) (Fig. 2*D*, right). This result showing Syt-7 depletion impairing release of RRP and

cognate islet SNARE and SNARE-associated proteins was not affected by the Syt-7-KD; Supplementary Fig. 1*B* shows the densitometric analysis of three experiments. Tubulin used as loading control; INS-1 (20 μg) and mouse brain (5 μg) are positive controls. *G*: Two examples (top and bottom images) showing effective downregulation of Syt-7 (green) expression in Ad-Syt-7–shRNA/RFP-infected (red) β-cells (blue). We deliberately chose areas with some residual Syt-7–positive cells, which are RFP negative as expected. Scale bars, 25 μm. *H*: Quantification of Ad-Syt-7–shRNA/RFP (red) infection efficiency of dispersed human islet cells (left) and KD efficiency of Syt-7 in dispersed β-cells (right). KD quantification was performed by comparing the most intensely green Syt-7 fluorescence indicating noninfected β-cells as 100 versus the amounts of residual Syt-7 green fluorescence in red cells. Values shown in (*D*) and (*H*) are means ± SEM. All data shown are representative of three independent experiments. $^{**}P < 0.01$, $^{***}P < 0.001$ by Student *t* test. + ve, positive; - ve, negative.

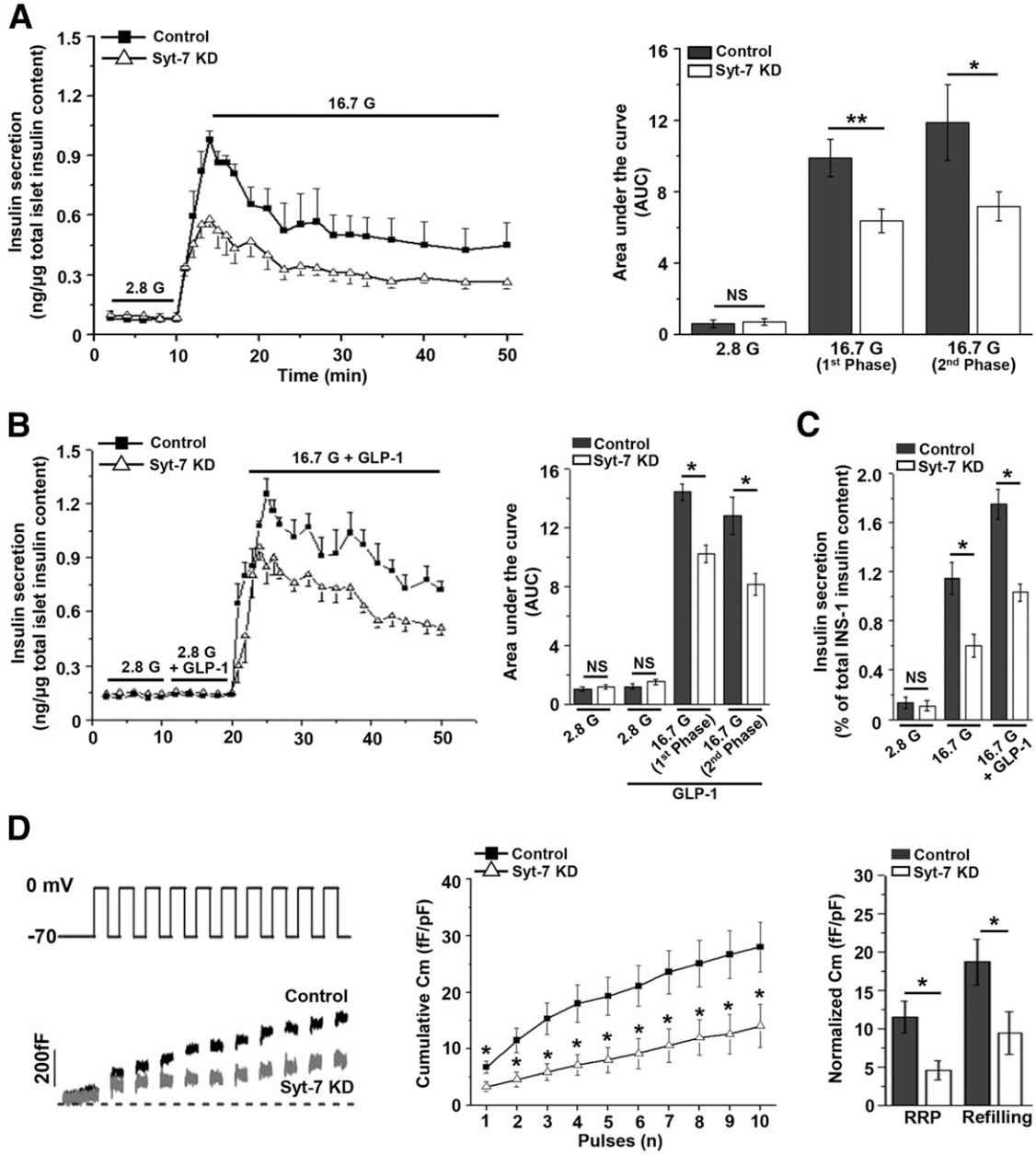

Figure 2—Syt-7 depletion in human islets reduces biphasic GSIS by its actions on releasable SG pools. High glucose (16.7 mmol/L) (*A*) and 10 nmol/L GLP-1 + 16.7 mmol/L glucose-stimulated (*B*) insulin secretion from isolated human islets transduced with Ad-*sc*-shRNA/RFP (control) or Ad-Syt-7-shRNA/RFP (Syt-7-KD). Insulin released was normalized to islet insulin content. Data shown are means ± SEMs from four different islet donors. Graphs on the right are area under the curve (AUC) analysis of first-phase (encompassing 11–22 min) and second-phase (encompassing 22–50 min) GSIS. *C*: Effect of Syt-7-KD on INS-1 cell GSIS. *D*: Left, representative capacitance recordings of single human β-cell exocytosis evoked by a train of ten 500-ms depolarizations (−70 to 0 mV) in control and Syt-7-KD human β-cells. Middle*:* cumulative changes in cell Cm normalized to basal cell Cm (fF/pF) in control (n = 13 cells) and Syt-7-KD (n = 10 cells) β-cells from two islet donors. Right: size of RRP of insulin SGs ($\Delta Cm_{1st–2nd\ pulse}$) and rate of SG mobilization ($\Delta Cm_{3rd–10th\ pulse}$) ($n$ = 10–13 cells). All values shown represent means ± SEM. *P < 0.05, **P < 0.01 by one-way ANOVA. G, mmol/L glucose.

mobilization of SGs from RP parallels the reduction in first- and second-phase GSIS (Fig. 2*A* and *B*).

Syt-7-KD Diminishes Biphasic GSIS by Reducing Exocytosis of Predocked and Newcomer SGs

Spatiotemporal mobilization of SGs and single SG fusion dynamics was assessed by time-lapsed TIRFM of SGs tagged with NPY-EGFP (11,17). Ad-NPY-EGFP was cotransfected into human β-cells along with control Ad-shRNA/RFP or Ad-Syt-7–shRNA/RFP. At basal state (2.8 mmol/L glucose), levels of punctuate fluorescence indicating docked SGs were not different between control (11.9 ± 0.448/100 μm^2) and Syt-7-KD β-cells (11.2 ± 0.582/100 μm^2) (Fig. 3*A*), consistent with the electron microscopy (EM) analyses (as shown

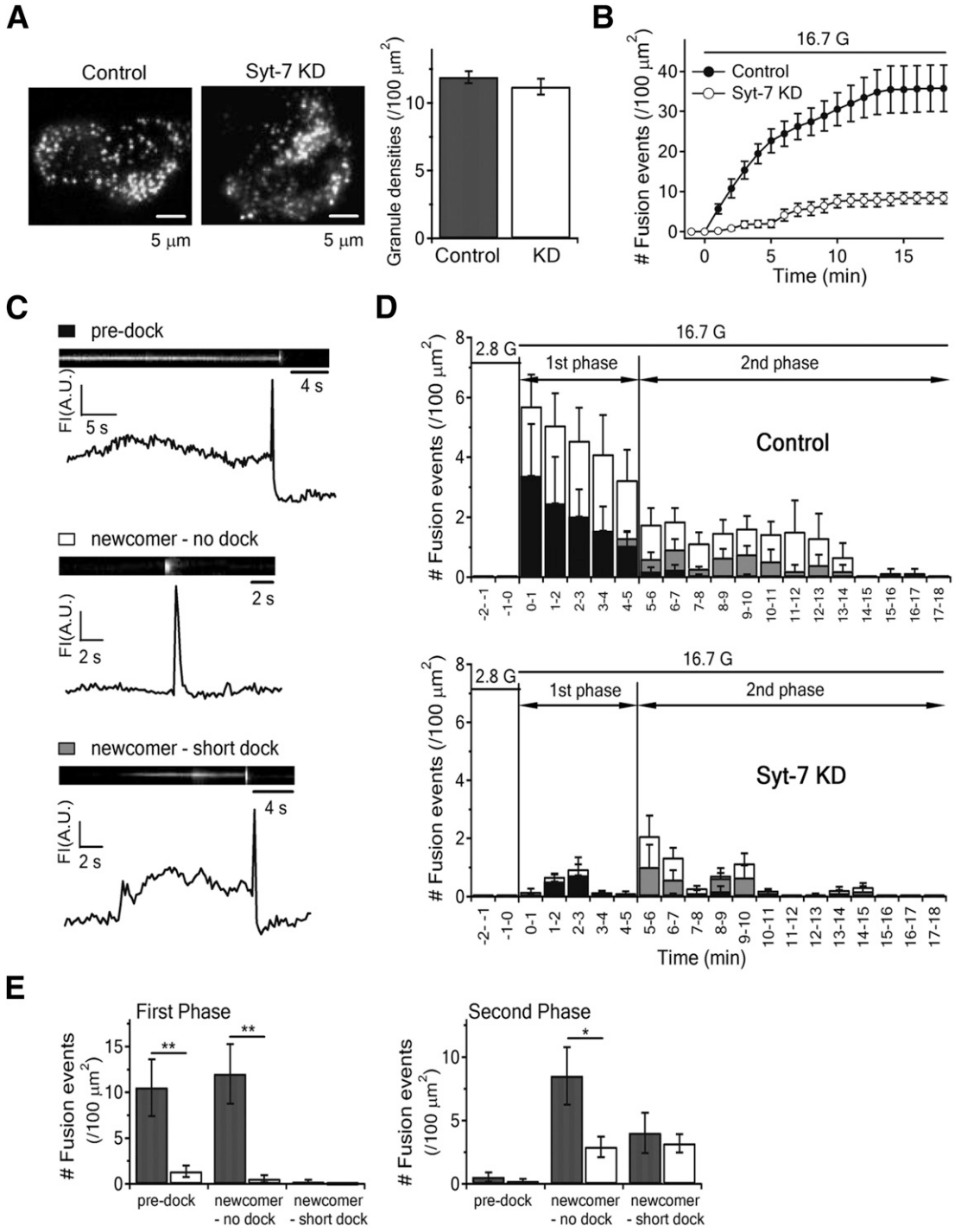

Figure 3—Syt-7 depletion diminishes biphasic GSIS by reducing exocytosis of predocked and newcomer SGs. *A*: TIRFM images of docked insulin SGs from control and Syt-7-KD human β-cells at basal (2.8 mmol/L glucose) condition (left: scale bars, 5 μm), which on analysis (right) showed no difference in SG density (means ± SEMs). *B*: Averaged cumulative fusion events of insulin SGs per cell per 100 μm^2 of PM surface stimulated as indicated. *C*: Representative kymographs and corresponding fluorescence intensity (FI) curves showing examples of the three modes of insulin SG fusion events. *D*: Histogram of the three patterns of fusion events: predock (black bar), newcomer-no dock (white bar), and newcomer-short dock (gray bar) in first phase (first 5 min after 16.7 mmol/L glucose stimulation) and second phase (5–18 min) in control (top) or Syt-7-KD (bottom) human β-cells. Time intervals for first and second phases are by convention as we previously reported (16,17,28,30). Data in *A–D* were obtained from three independent experiments (two to four cells from each islet donor, three islet donors) (control: 9 cells; Syt-7-KD: 10 cells), expressed as means ± SEMs. *E*: Summary of the three patterns of fusion events in first phase (left) and second phase (right), shown as means ± SEMs. $^*P < 0.05$, $^{**}P < 0.01$. A.U., arbitrary units; G, mmol/L glucose.

in Fig. 6E). With 16.7 mmol/L glucose stimulation, single SG fusion events were observed as flashes of fluorescence that rapidly dissipated in a cloudlike diffusion pattern. Assessment of cumulative fusion events over time (Fig. 3*B*) showed far fewer fusion events during the 18-min stimulation in Syt-7-KD β-cells than control β-cells. These exocytotic events are not uniform but display three distinct modes (7,10). Predock SG fusion (Fig. 3*C*, top) (black in Fig. 3*D*) refers to SGs that were already docked onto the PM prior to stimulation. Newcomer SGs are SGs appearing de novo under the evanescent field after stimulation that then undergo exocytosis after a short period of residence time at the PM varying from seconds to minutes (called newcomer-short dock SGs) (Fig. 3*C*, bottom) (gray in Fig. 3*D*) or immediately fuse with PM (called newcomer-no dock SGs) (Fig. 3*C*, middle) (white in Fig. 3*D*) with a docking state of <200 ms (minimal interval between two consecutive frames). We assessed these three modes of fusion events impacted by the Syt-7-KD.

In first-phase GSIS, newcomer SGs accounted for >50% of exocytotic events in control β-cells (Fig. 3*D*, top). In this study, we found in Syt-7-KD β-cells very major reduction of fusion events (summary analysis, Fig. 3*E*) attributed to both predock (control: 10.50 ± 3.10; Syt-7-KD: 1.38 ± 0.62/100 μm^2) and newcomer-no dock SGs (control: 12.02 ± 3.26; Syt-7-KD: 0.59 ± 0.37/100 μm^2). These results suggest that in basal state in Syt-7–depleted β-cells, insulin SGs are still able to dock onto the PM; however, Syt-7 depletion caused a loss of fusion competence of these predock SGs during stimulation. In second-phase GSIS, exocytosis of only the much larger population of newcomer-no dock SG fusion was reduced (control: 8.51 ± 2.27; Syt-7-KD: 2.93 ± 0.80/100 μm^2) (summary analysis in Fig. 3*E*). This suggests that Syt-7-KD either caused a fusion defect and/or reduced recruitment of newcomer SGs to the PM after stimulated depletion.

Syt-7-C2AB Domain Interacts With Syn-1A and Syn-3 in a Ca^{2+}-Dependent Manner to Promote SNARE Complexes on Stimulation

To examine whether Syt-7 exerts its functions in β-cell insulin SG exocytosis by interactions with syntaxins, we performed coimmunoprecipitation (co-IP) assays with INS-1 cells at basal state (0.8 mmol/L glucose) and maximal stimulatory conditions (preincubation with cAMP-acting 10 nmol/L GLP-1 followed by 16.7 mmol/L glucose) using Syn-1A (Fig. 4*A*) and Syn-3 antibodies (Fig. 4*C*). INS-1 (not human islets) provides an abundance of proteins required for this assay. IPs recovered equivalent amounts of Syn-1A and Syn-3 in both basal state and glucose-stimulated cells (Syn-1A, basal: 14.4 ± 2.1%, stimulated: 15.05 ± 2.3%, and Syn-3, basal: 14.25 ± 1.5, stimulated: 14.9 ± 1.9) (Fig. 4*B* and *D*); this reflects the intrinsic affinities of antibodies for endogenous syntaxins not affected by stimulation. Glucose stimulation resulted in ~115% increase in Syt-7 association with Syn-1A (basal: 3.8 ± 0.9 vs. stimulated: 8.2 ± 1) (Fig. 4*B*) and a larger ~335% increase in Syt-7 association with Syn-3 (basal: 2.84 ± 0.9 vs. stimulated: 12.26 ± 1.7) (Fig. 4*D*). There were consistent increases in SNAP25 (Syn-1A: ~342%, Syn-3: ~257%) and preferential binding of VAMP2 and VAMP8 by Syn-1A and Syn-3, respectively. First, these results confirm the increase in formation of distinct SNARE complexes after glucose stimulation as previously reported (15,17). Second, stimulation of β-cells induced an increased association of Syt-7 with Syn-1A–SNARE complex (Syn-1A/VAMP2/SNAP25) postulated to mediate fusion of predocked SGs. This result is further proof supporting our previous report using an in vitro fusion assay that Syt-7 facilitated Syn-1A–SNARE complex–mediated fusion (35). Third, most important and novel, is an increase in association of Syt-7 with Syn-3–SNARE complex (Syn-3/VAMP8/SNAP25) (Fig. 4*C* and *D*) that we had reported to mediate exocytosis of newcomer SGs (7,15–17).

To determine whether Syt-7 co-IP with Syn-1A and Syn-3 is due to direct interactions at its C2A and/or C2B domains, pulldown assays using GST proteins of these domains on HEK cells expressing Syn-1A (Fig. 4*E* and *F*) or Syn-3 (Fig. 4*G* and *H*) showed that GST-C2AB (residues 134–403 linking C2A and C2B), C2A (residues 134–263), and C2B (residues 243–403) domains bound both Syn-3 and Syn-1A. In this study, Syt-7-C2B binds both syntaxins more strongly than C2A (Fig. 4*E* and *G*). We determined if C2AB binding to Syn-1A and Syn-3 is Ca^{2+}-dependent by using a Syt-7 Ca^{2+}-binding mutant C2AB-4D/N (C2A-2D/N:D225,227N; C2B-2D/N:D357,359N) (36). In absence of Ca^{2+}, GST-C2AB wild-type brought down small amounts of Syn-1A (Fig. 4*F*) and Syn-3 (Fig. 4*H*), whereas presence of Ca^{2+} brought down an abundance of both syntaxins. In contrast, GST-C2AB-4D/N mutant bound very little amounts of_Syn-1A and Syn-3 in absence or presence of Ca^{2+}. These results demonstrating that Syt-7 binding to Syn-1A and Syn-3 increased in a Ca^{2+}-dependent manner (Fig. 4*F* and *H*) suggest that Syt-7 acts as Ca^{2+} sensor for the Syn-1A–SNARE complex to mediate predocked SG exocytosis and Syn-3–SNARE complex to mediate newcomer SG exocytosis. Consistently, we had reported using an in vitro fusion assay that Syt-7 facilitated Syn-1A–SNARE complex-driven fusion that was also Ca^{2+} dependent (35).

Syt-7 Depletion Does Not Disrupt Glucose-Stimulated SNARE Complex Assembly

We next assessed whether Syt-7 depletion influences SNARE complex formation per se that underlies exocytosis of predocked and newcomer SGs. We conducted co-IPs with Syn-1A or Syn-3 antibodies on control (Ad-*sc*-shRNA/RFP) and Syt-7-KD (Ad-Syt-7–shRNA/RFP-infected) INS-1 at nonstimulatory and maximal stimulatory conditions (Fig. 5). Syt-7-KD with Ad-Syt-7–shRNA/RFP was optimized (Supplementary Fig. 3*A*) and verified in INS-1 cells intended for co-IP (Supplementary Fig. 3*C*), which was consistently >78% reduction; Syt-7 expression was confirmed to not change in control cells (Supplementary Fig. 3*B*). Under nonstimulatory conditions, Syn-1A (Fig. 5*A*)

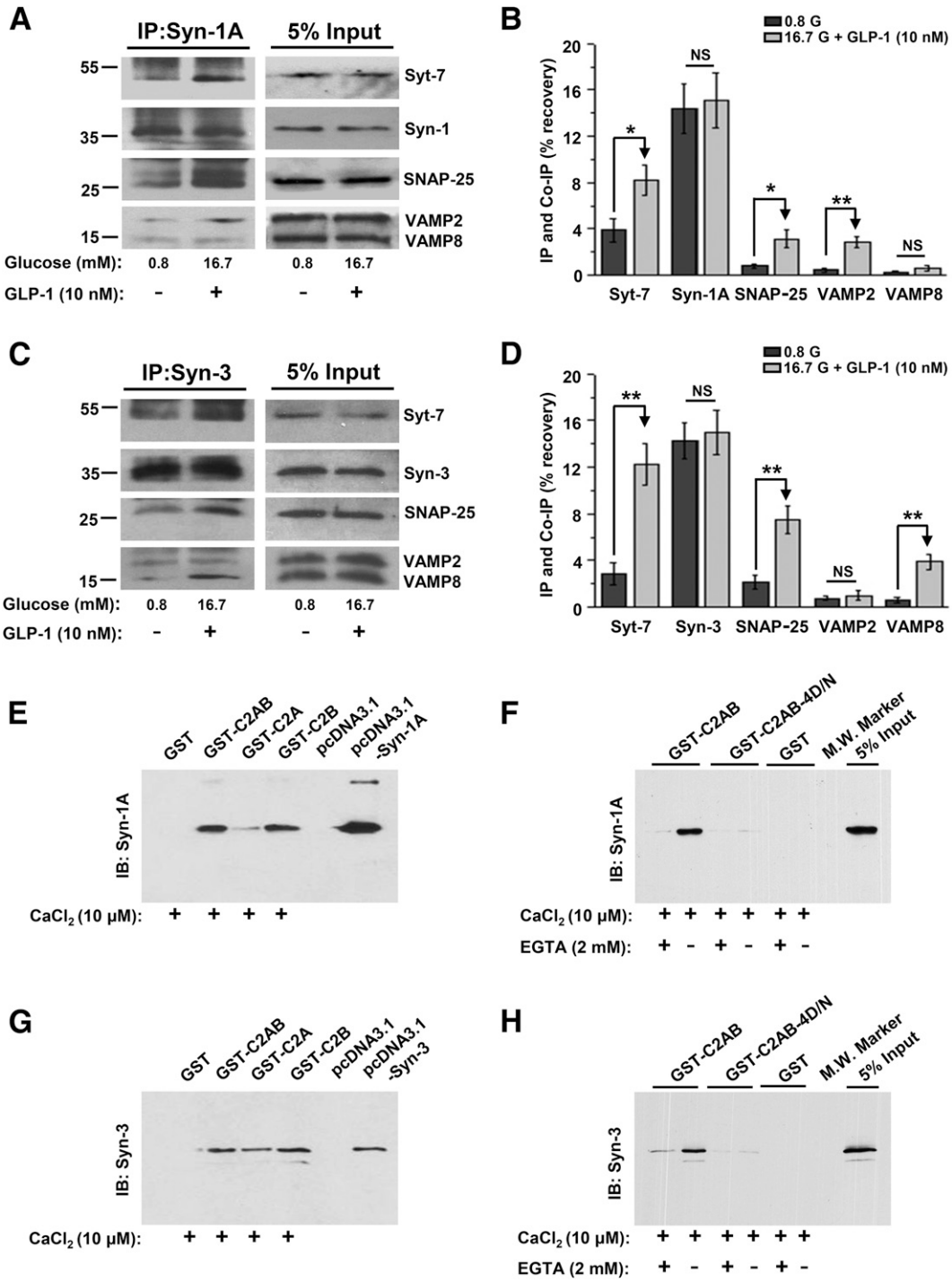

Figure 4—Syt-7 at its C2AB domain interacts with Syn-1A and Syn-3 in β-cells in a Ca^{2+}-dependent manner to promote their respective SNARE complexes upon glucose stimulation. Syt-7 coimmunoprecipitates with Syn-1A (*A*) and Syn-3 (*C*) upon glucose stimulation of INS-1 cells. INS-1 cells were kept in either nonstimulatory condition (0.8 mmol/L glucose) or stimulated with 16.7 mmol/L glucose + 10 nmol/L GLP-1. Total of 500 μg proteins from each condition were subjected to IP (left) with antibody against Syn-1A or Syn-3 and probed with indicated antibodies. Corresponding right panels show 5% input controls (25 μg protein, total INS lysates), confirming the similar expression levels of these proteins (analyses in Supplementary Fig. 2*A* and *B*). Results shown are representative of five independent experiments. *B* and *D* are the quantitations of IP and co-IP proteins with Syn-1A and Syn-3, respectively. Shown as means ± SEMs. We then show that Syn-1A (*E* and *F*) and Syn-3 (*G* and *H*) interactions with Syt-7 are Ca^{2+} dependent. HEK293 cells were transfected with Syn-1A or Syn-3. GST (negative control), GST-C2AB, GST-C2A, and GST-C2B (*E* and *G*) and GST-C2AB-4D/N Ca^{2+}-binding mutant (*F* and *H*), all bound to agarose glutathione beads, were used to pull down the overexpressed syntaxins (400 μg HEK cell protein). Syn-transfected and empty vector–transfected HEK cell lysate extracts (20 μg protein) were used as positive and negative controls. Data are representative of three independent experiments showing identical results. Ponceau-S–stained blots of these experiments in *E–H* show equivalent loading of individual GST-tagged proteins as shown in Supplementary Fig. 2*C–F*. $^*P < 0.05$, $^{**}P < 0.01$. G, mmol/L glucose; IB, immunoblot.

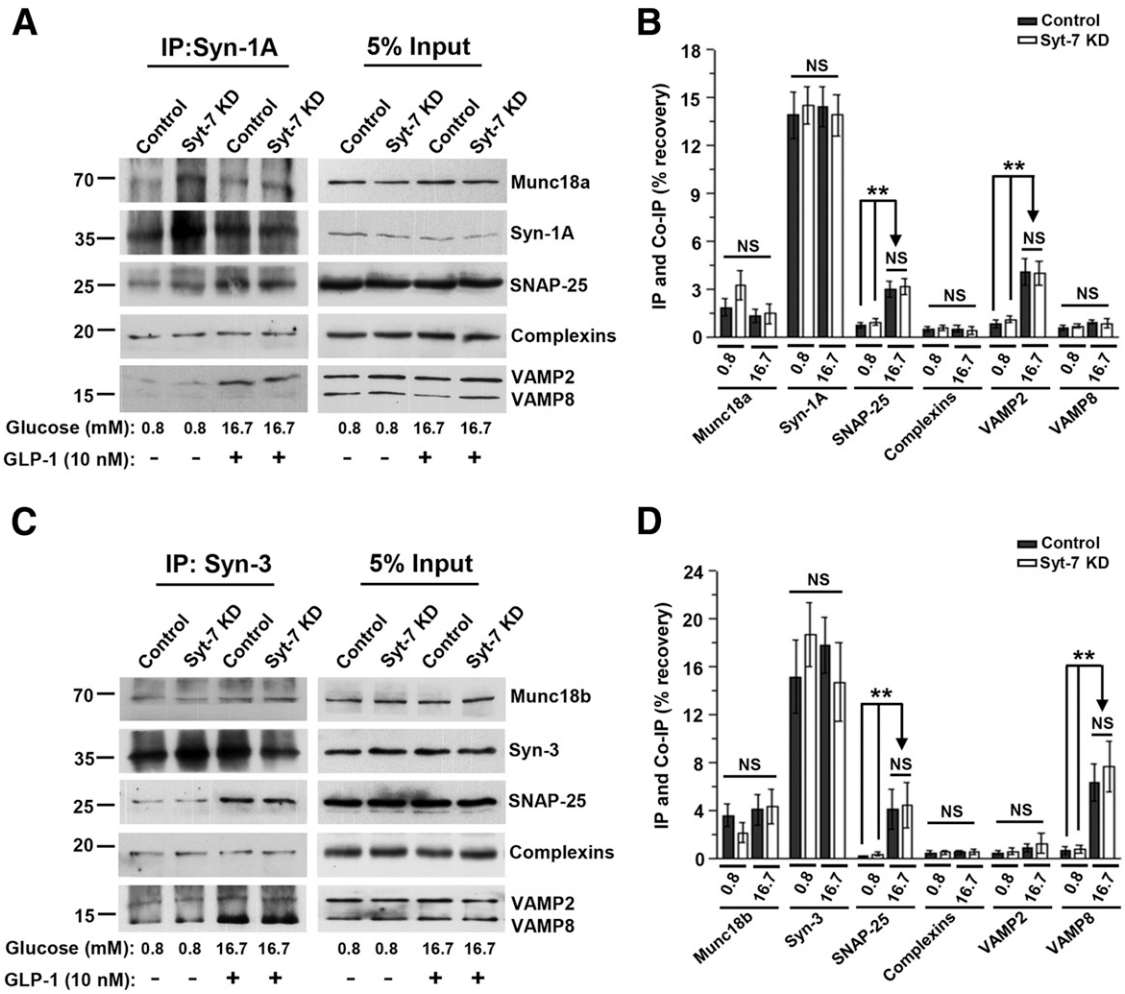

Figure 5—Syt-7 depletion does not disrupt glucose-stimulated SNARE complex assembly. INS-1 cells were transduced with Ad-Syt-7-shRNA/RFP or control Ad-*sc*-shRNA/RFP for 48 h, then kept at basal condition (0.8 mmol/L glucose) or stimulated with 16.7 mmol/L glucose plus 10 nmol/L GLP-1, and then subjected to IP with antibodies against Syn-1A (*A*) or Syn-3 (*C*). Corresponding right panels showing 5% input controls (25 μg protein, total INS-1 lysates) confirmed the similar levels of indicated SNARE proteins (analyses in Supplementary Fig. 3*D* and *E*). Results shown are representative of five independent experiments, with their analysis shown in *B* for Syn-1A IP and *D* for Syn-3 IP. Representative blot showing reduction in Syt-7 expression in Ad-Syt-7-shRNA/RFP-transduced cells and the densitometry analyses of the inputs are in Supplementary Fig. 3*C*. $^{**}P < 0.01$.

and Syn-3 (Fig. 5*C*) bound similarly little SNAP25 and VAMPs (VAMP2 and VAMP8) in control and Syt-7–depleted INS-1. Upon glucose stimulation, which activates SNARE complex assembly (Fig. 4*A* and *C*), there was increased SNARE complex formation, with Syn-1A preferring to bind VAMP2 (Fig. 5*A*) and Syn-3 preferring VAMP8 (Fig. 5*C*). In Syt-7–depleted INS-1, Syn-1A and Syn-3 antibodies coprecipitated similarly increased amounts of SNAP25 as control cells (Syn-1A, control: 2.9 ± 0.48, Syt-7-KD: 3.1 ± 0.52%; Syn-3, control: 4.06 ± 1.24%, Syt-7-KD: 4.19 ± 1.46%). In addition, between control and Syt-7–depleted INS-1, Syn-1A coprecipitated similarly increased amounts of VAMP2 (control: 4.0 ± 0.82%; Syt-7-KD: 3.94 ± 0.7%); Syn-3 coprecipitated similarly increased amounts of VAMP8 (control: 6.29 ± 1.59%; Syt-7-KD: 7.18 ± 1.63%). Because complexin acts in concert with Syt-7 on the SNARE complex (37), we found that Syn-1– and Syn-3–SNARE complexes indeed brought down complexin but complexin levels did not increase with glucose stimulation and were not affected by Syt-7 depletion (Fig. 5*A* and *C*). These results demonstrate that Syt-7 depletion, while potently blocking exocytosis (Figs. 2 and 3), had remarkably no effect on stimulation-induced increase in SNARE complex assembly. This is surprising, as we expected Syt-7 depletion to disrupt or destabilize SNARE complex assembly. This result indicates that Syt-7 actions on insulin SG exocytosis might not require Syt-7–driven SNARE complex assembly, but rather Syt-7 might act at a more distal step after SNARE complexes have assembled, at the level of fusion perhaps (38).

Syt-7 Acts With Calmodulin to Recruit Insulin SGs to PM to Replenish Depleted Pools From Glucose Stimulation

Although TIRFM is excellent at examining behavior of SGs close to the PM (up to 100 nm), we wanted to also

assess insulin SG behavior further inside the cytoplasm—in particular, whether SGs are adequately recruited to the PM to replenish the pools of SGs near the PM that have been depleted by glucose-stimulated exocytosis. This required EM morphometric analysis of control and Syt-7-KD β-cells at basal and after 16.7 mmol/L glucose stimulation (Fig. 6*A*). β-Cells near the islet periphery were chosen, as they are most likely to be infected by Ad-Syt-7–shRNA and thus reliably depleted of Syt-7. There was no difference in total number of SGs by which relative SG densities between control and Syt-7-KD β-cells were comparable (Fig. 6*D* and *F*) at basal state. SG diameters were also similar (control: 256.492 ± 3.13 nm; Syt-7-KD: 257.176 ± 3.10 nm, from six independent donors), indicating that Syt-7 did not affect insulin SG biogenesis. At basal state, the number of morphologically docked SGs at the PM (SG center ≤100 nm distance from PM) (39) were similar between control and Syt-7-KD β-cells (Fig. 6*E*,*1*).

We then examined the ability of insulin SGs to mobilize to the PM after 16.7 mmol/L glucose-stimulated depletion of the releasable pools. Glucose stimulation was for 15 min to encompass biphasic GSIS for single β-cells (like TIRFM study) (Fig. 3) and then immediately fixed; SG distribution was then assessed by determining the number of morphologically docked SGs (Fig. 6*E*) and SG densities within 0.2-μm concentric shells beneath the PM (Fig. 6*F*) (29). At basal state, SG density within each shell expressed as the percentage of average density of total cytoplasmic SGs within 1.5 μm from the PM (29) was similar at every concentric shell between control and Syt-7-KD β-cells (compare top images in Fig. 6*A*; analysis in Fig. 6*F*). After 16.7 mmol/L glucose stimulation, we saw a major increase in SGs moving toward the PM (within 0.2 μm) in control cells (bottom left in Fig. 6*A*; analysis in Fig. 6*F*) as well as an increase in morphologically docked SGs (Fig. 6*E*) (2.8 mmol/L glucose: 11.25 ± 1.86, 16.7 mmol/L glucose: 13.25 ± 1.78), indicating efficient SG recruitment to replenish depleted releasable SG pools and sustain second-phase GSIS. However, this recruitment of SGs to PM was much reduced in Syt-7-KD cells after 16.7 mmol/L glucose stimulation, in which we saw obvious paucity of SGs in many areas beneath the PM, some for two to three SG diameters (bottom right image in Fig. 6*A*). Morphometric analysis showed 56% reduction in morphologically docked SGs (Fig. 6*E*) (control: 13.25 ± 1.78, Syt-7-KD: 5.8 ± 1.32), 42.9% decrease in SG number at 0–0.2 μm beneath the PM (control: 148.62 ± 13.65%; Syt-7-KD: 84.94 ± 7.58), and 32.2% decrease at 0.2–0.4 μm beneath the PM (control: 132.76 ± 14.59%; Syt-7-KD: 90.08 ± 6.64%). Further into the cell interior in control cells that showed the expected progressive reduction of SG density, every concentric shell from 0.4 to 1.5 μm from the PM in Syt-7-KD cells instead showed more SGs than regions close to the PM. This indicates that Syt-7 depletion severely restrained the trafficking of insulin SGs from the cell interior to the PM after stimulated depletion of releasable SG pools situated just beneath the PM. This defect in replenishment of SGs during stimulation we postulate to largely account for the reduced refilling of RRP in the Cm study (Fig. 2*D*) and reduced rate of exocytosis of newcomer SGs in the TIRFM study (Fig. 3*E*).

Syt-7 was recently reported to be a putative exocytotic substrate for GLP-1 in potentiating GSIS (22). We therefore assessed whether GLP-1 could surmount the Syt-7-KD–mediated defect in SG recruitment (Fig. 6*B*). Whereas GLP-1 pretreatment followed by 16.7 mmol/L glucose stimulation resulted in some increase in the number of morphologically docked SGs (Fig. 6*E*, compare *2* and *3*) and SGs mobilized to the 0–0.2 μm and 0.2–0.4 μm concentric rings (Fig. 6*F*, compare *2* and *3*) compared with 16.7 mmol/L glucose alone, Syt-7-KD resulted in similar reductions of 53% in the morphologically docked SGs, 40.5% in SG density within 0–0.2 μm, and 28% within 0.2–0.4 μm beneath the PM. This likely explains the failure of GLP-1 to rescue the deficient biphasic GSIS caused by Syt-7 depletion (Fig. 2*B*).

Very little is known about the molecular machinery of SG recruitment from the cell interior. In our recent report (36), we had surmised the possibility that calmodulin (CaM) reported to affect synaptic vesicle recruitment (40) might act in concert with Syt-7 (36). At basal state, CaM antagonist calmidazolim (Cmdz) pretreatment did not affect SG distribution (Fig. 6*C*–*F*). However, after 16.7 mmol/L glucose (*2* in Fig. 6*E* and *F*) or 10 nmol/L GLP-1 + 16.7 mmol/L glucose stimulation (*3* in Figs. 6*E* and *F*), the effects of Cmdz pretreatment (Fig. 6*C*) on insulin SG recruitment to the PM were reduced to an extent remarkably similar to that in Syt-7-KD β-cells. These results suggest a requirement for CaM by Syt-7 in the recruitment of SGs to the PM in human β-cells.

DISCUSSION

We demonstrated the different roles of Syt-7 in insulin SG exocytosis in human β-cells. Depletion of Syt-7 in human pancreatic islets inhibited first- and second-phase GSIS, which, on Cm experiments, was shown to be attributed to reduction in RRP and refilling of RRP from RPs (Fig. 2) and, on TIRFM, was shown to be attributed to reduction of newcomer-no dock SGs in first- and second-phase GSIS (Fig. 3) and reduction of predocked SGs in first-phase GSIS. Syt-7 is therefore a positive regulator of exocytosis of both pools of predocked and newcomer SGs underlying biphasic GSIS.

Insulin SGs are functionally segregated into RRP and RPs, by which primed predocked SGs are major contributors to RRP and a major portion of first-phase GSIS, whereas newcomer SGs from RPs contribute to second-phase GSIS. Predocked SGs require formation of excitosome complexes with L-type Ca_vs (41) to access the high Ca^{2+} concentrations coming through Ca_vs acting on a lower Ca^{2+}-affinity Ca^{2+} regulator that triggers predocked SM/SNARE complexes to complete the fusion process (14). More Ca^{2+}-sensitive newcomer SGs respond to bulk Ca^{2+} influx arising from *R*-type Ca_vs (14,42), suggesting a requirement for a high-affinity Ca^{2+} regulator for the newcomer SG SM/SNARE complex

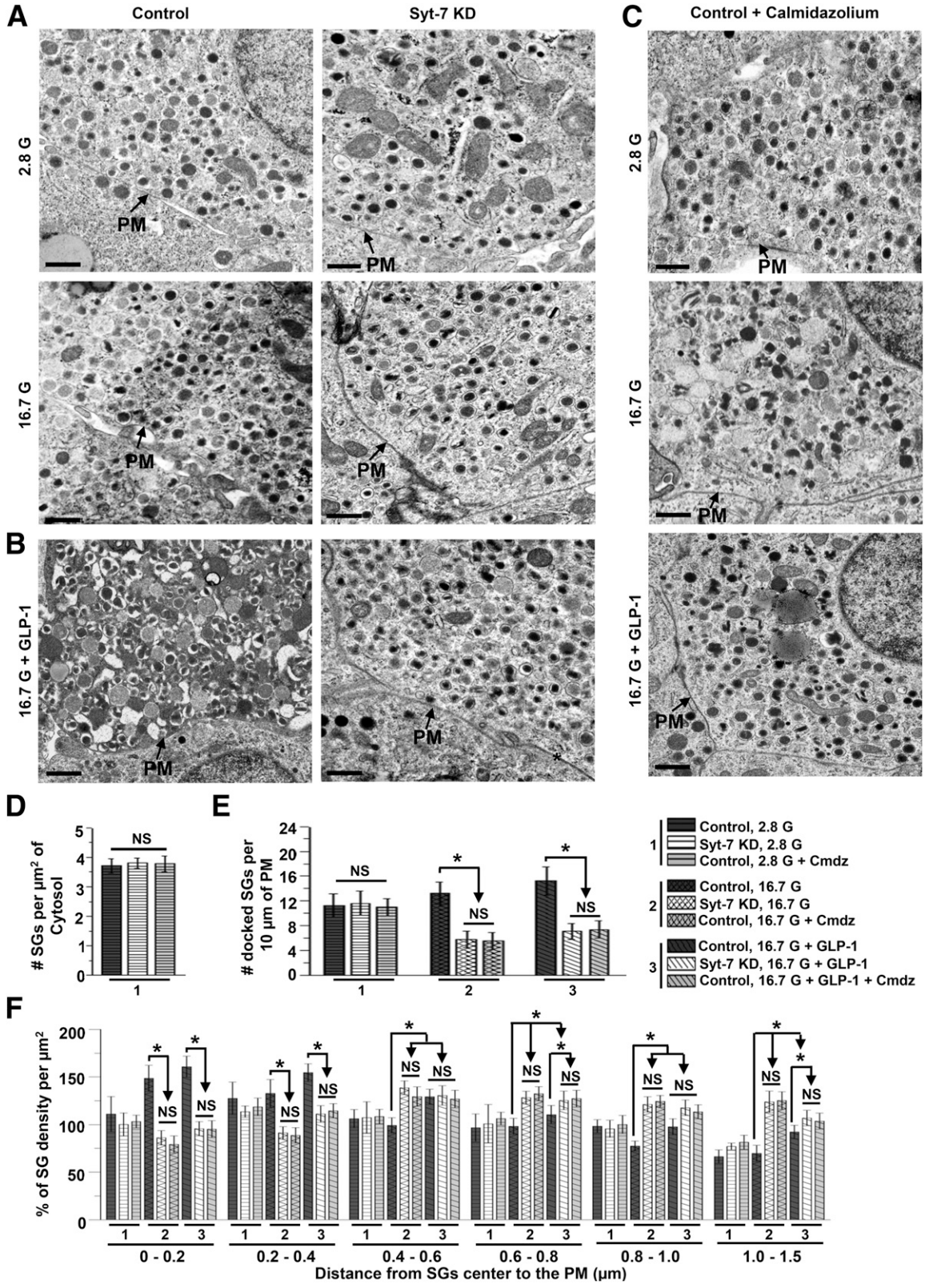

Figure 6—Syt-7 recruits insulin SGs to the PM to replenish depleted pools from glucose stimulation. *A*: Representative electron micrographs of basal (2.8 mmol/L glucose [G], top) and 16.7 mmol/L glucose-stimulated (for 15 min, bottom) control (left) and Syt-7-KD (right) human islets. *B*: Representative electron micrographs of 10 nmol/L GLP-1–potentiated, 16.7 mmol/L glucose-stimulated control (left) and Syt-7-KD (right) human islets. *C*: Representative electron micrographs of the effects of CaM antagonist Cmdz (20 μmol/L) pretreatment of control human islets on basal (2.8 mmol/L glucose, top), 16.7 mmol/L glucose stimulation (for 15 min, middle), and 10 nmol/L GLP-1–potentiated 16.7 mmol/L glucose stimulation (for 15 min, bottom). Arrows indicate the PM. Scale bars, 0.5 μm. *D*: Total SG number/μm^2 of the total cytoplasmic area; $n = 24$ micrographs each for control and Syt-7-KD islets and 10 micrographs for Cmdz-treated islets, from six

(14). As this would suggest two different Ca^{2+} sensors, we were surprised that Syt-7 acted as Ca^{2+} sensor for both low Ca^{2+}-affinity predocked SGs and high Ca^{2+}-affinity newcomer SGs. Consistently, newcomer SGs also displayed high sensitivity to Munc13-1 (30), cAMP effectors GEF2 and Rim2a (9,10), and SG-tethering factor Sec5 (28), which altogether suggest that Syt-7 would likewise sensitize newcomer SGs to become fusion competent. This perhaps in part explains why newcomer SGs require little residence time at the PM before fusion.

We assessed Syt-7 interaction with Syn-1A and Syn-3 that underlie the assembly of respective exocytic SNARE complexes for predocked and newcomer SGs. Remarkably, both Syt-7/SNARE complexes increased with glucose stimulation (Fig. 4). Syt-7, like Syt-1, might act as a fusion clamp that arrests SNARE-catalyzed fusion at the PM in β-cells, and this clamp becomes relieved by the Ca^{2+} trigger (3,43). We dissected the major interacting domains of Syt-7 and observed that both C2A and C2B bind Syn-1A and Syn-3, but more avid binding was observed with the C2B domain. Ca^{2+}-binding mutant C2AB-4D/N (36) exhibited a similarly small amount of binding to both Syns in absence or presence of Ca^{2+}, indicating some degree of Ca^{2+}-independent interaction. In contrast, wild-type C2AB bound small amounts of both Syns in absence of Ca^{2+}, and Ca^{2+} then greatly promoted C2AB binding to both Syns. These results indicate that Syt-7 acts as a Ca^{2+} sensor for exocytosis of predocked and newcomer SGs through C2AB interactions with Syn-1A and Syn-3, respectively. Because Syn-3 binding to C2B was noticeably stronger than Syn-1A, Syt-7–Syn-3 structural-functional interactions may be different from Syt-7–Syn-1A interactions (44,45), which require further studies.

Surprisingly, Syt-7 depletion, although severely reducing insulin SG exocytosis, did not affect glucose-stimulated increase in SNARE complex assembly (Fig. 5), suggesting several possibilities: *1*) compensatory actions of another Syt(s) or 2) Syt-7's actions on exocytosis might be SNARE independent. Other Syts present in β-cells (20) could promote SNARE complex assembly and compensate for loss of Syt-7. Whereas Syt-9 is the next most abundant Syt in β-cells, loss of Syt-9 did not affect GSIS or glucose homeostasis (46). Syts, particularly Syt-7, have strong interactions with PM phospholipids that promote higher frequency of fusion events and more stable fusion pores that were remarkably uncorrelated to Syt-induced SNARE protein assembly (38). Taken together, Syt-7s may mediate insulin SG fusion at the PM by Syt-7–driven *t*-SNARE assembly and/or Syt-7–PM phospholipids interactions. It appears that the latter may be more important, because insulin SGs in Syt-7-KD β-cells remained able to morphologically dock at the PM during basal state (by TIRFM and EM), but these predocked SGs lost their fusion competence when stimulated (Fig. 3).

A third possibility is that Syt-7 acts to replenish SGs, which is required after high-frequency or sustained stimulation, as we have reported to occur in neurons (36). We showed that Syt-7 has similar actions in β-cells in which Syt-7-KD caused reduction in recruitment of insulin SGs from the cell interior to the PM after a 15-min glucose stimulation, leading to SGs accumulation further into the cell interior (Fig. 6). This resulted in reduced newcomer SGs and consequent reduced capacity to sustain second-phase GSIS. However, at rest (basal condition), SGs in Syt-7-KD β-cells were able to eventually get to the PM, which explains the similar number of docked SGs as in control cells. The latter indicates that Syt-7-KD reduces the efficiency but does not block SG recruitment to the PM. Our data support the possibility that this role in SG recruitment to the PM by Syt-7 could be mediated by Syt-7 formation of a complex with CaM (36) rather than with *t*-SNAREs. CaM was found to interact with Munc13-1 to regulate SV replenishment (40). Syt-7, along with CaM and Munc13-1, might thus act in concert to replenish insulin SGs to supply the RPs after glucose-stimulated depletion. This might in part explain why depletion of Syt-7 (this study) or Munc13-1 (30) had such big effects on newcomer SGs. If the predominant action of Syt-7 is interaction with *t*-SNAREs on PM, then the Ca^{2+}-sensing defect from the loss of Syt-7 would have resulted in accumulation of SGs at or close to the PM, which was not the case in this study. Taken together, our results support a major role for Syt-7 in recruitment of insulin SGs to the PM required to sustain secretion with continued stimulation. This mode likely also occurs in adrenal chromaffin cells (45). Much further work will be required to elucidate the full molecular basis.

Levels of SNARE and priming proteins in human type 2 diabetes (T2D) β-cells are severely reduced (23,24), which in part explains the reduction of exocytosis of predocked SGs. The SNARE exocytotic machinery mediating newcomer SGs might also be defective in T2D. Interestingly, Syt-7 levels are also reduced in human T2D β-cells (23). Even with defective SNARE machineries in T2D β-cells, restoring/increasing Syt-7 expression might still be able to increase the replenishment and/or fusion efficiency of both predocked and newcomer SGs, as well as

different islet donors. *E*: Quantitative analysis of morphologically docked SGs in human β-cells. *F*: Relative density of SGs within 0.2-μm concentric shells below the PM. Data shown are percentages of SG density within each concentric shell relative to the average SG density in the total cytoplasm within 1.5 μm from the PM. For *E* and *F*, $n = 10$ micrographs for every condition from three independent experiments; islets were from six different donors. Data in *D–F* are represented as mean values ± SEM. Statistical analysis was by Student *t* test. $^*P < 0.05$.

amplify the efficacy of GLP-1–based drugs (33) to more effectively treat patients with T2D.

Funding. This work was supported by the Canadian Institutes of Health Research (CIHR) (grants MOP86544 and MOP89889). S.D. is funded by a postdoctoral fellowship from the Canadian Association of Gastroenterology and CIHR. Some equipment used in this study was supported by the 3D (Diet, Digestive Tract and Disease) Centre funded by the Canadian Foundation for Innovation and Ontario Research Fund, project number 19442.

Duality of Interest. No potential conflicts of interest relevant to this article were reported.

Author Contributions. S.D. formulated the original hypothesis, drafted the manuscript, and performed protein binding, EM, and INS-1 insulin secretion studies. L.X. performed electrophysiology and confocal studies. D.Z. performed TIRFM. T.L. performed confocal studies. T.Q. performed islet perifusion. H.X. and Y.K. performed expression and purification of recombinant proteins. E.R.C. provided key reagents and edited the manuscript. H.Y.G. formulated the original hypothesis and drafted the manuscript. All authors discussed the results. H.Y.G. is the guarantor of this work and, as such, had full access to all the data in the study and takes responsibility for the integrity of the data and the accuracy of the data analysis.

References

1. Südhof TC, Rothman JE. Membrane fusion: grappling with SNARE and SM proteins. Science 2009;323:474–477
2. Bhalla A, Chicka MC, Tucker WC, Chapman ER. Ca(2+)-synaptotagmin directly regulates t-SNARE function during reconstituted membrane fusion. Nat Struct Mol Biol 2006;13:323–330
3. Chapman ER. How does synaptotagmin trigger neurotransmitter release? Annu Rev Biochem 2008;77:615–641
4. Rorsman P, Renström E. Insulin granule dynamics in pancreatic beta cells. Diabetologia 2003;46:1029–1045
5. Kwan EP, Gaisano HY. Rescuing the subprime meltdown in insulin exocytosis in diabetes. Ann N Y Acad Sci 2009;1152:154–164
6. Gaisano HY. Deploying insulin granule-granule fusion to rescue deficient insulin secretion in diabetes. Diabetologia 2012;55:877–880
7. Gaisano HY. Here come the newcomer granules, better late than never. Trends Endocrinol Metab 2014;25:381–388
8. Kasai K, Fujita T, Gomi H, Izumi T. Docking is not a prerequisite but a temporal constraint for fusion of secretory granules. Traffic 2008;9:1191–1203
9. Seino S, Shibasaki T, Minami K. Dynamics of insulin secretion and the clinical implications for obesity and diabetes. J Clin Invest 2011;121:2118–2125
10. Shibasaki T, Takahashi H, Miki T, et al. Essential role of Epac2/Rap1 signaling in regulation of insulin granule dynamics by cAMP. Proc Natl Acad Sci USA 2007;104:19333–19338
11. Ohara-Imaizumi M, Nakamichi Y, Tanaka T, Ishida H, Nagamatsu S. Imaging exocytosis of single insulin secretory granules with evanescent wave microscopy: distinct behavior of granule motion in biphasic insulin release. J Biol Chem 2002;277:3805–3808
12. Barg S, Ma X, Eliasson L, et al. Fast exocytosis with few Ca(2+) channels in insulin-secreting mouse pancreatic B cells. Biophys J 2001;81:3308–3323
13. Henquin JC, Ishiyama N, Nenquin M, Ravier MA, Jonas JC. Signals and pools underlying biphasic insulin secretion. Diabetes 2002;51(Suppl. 1):S60–S67
14. Pedersen MG, Sherman A. Newcomer insulin secretory granules as a highly calcium-sensitive pool. Proc Natl Acad Sci USA 2009;106:7432–7436
15. Lam PP, Ohno M, Dolai S, et al. Munc18b is a major mediator of insulin exocytosis in rat pancreatic β-cells. Diabetes 2013;62:2416–2428
16. Zhu D, Koo E, Kwan E, et al. Syntaxin-3 regulates newcomer insulin granule exocytosis and compound fusion in pancreatic beta cells. Diabetologia 2013;56:359–369
17. Zhu D, Zhang Y, Lam PP, et al. Dual role of VAMP8 in regulating insulin exocytosis and islet β cell growth. Cell Metab 2012;16:238–249
18. Gauthier BR, Wollheim CB. Synaptotagmins bind calcium to release insulin. Am J Physiol Endocrinol Metab 2008;295:E1279–E1286
19. Gao Z, Reavey-Cantwell J, Young RA, Jegier P, Wolf BA. Synaptotagmin III/VII isoforms mediate Ca2+-induced insulin secretion in pancreatic islet beta -cells. J Biol Chem 2000;275:36079–36085
20. Gauthier BR, Duhamel DL, Iezzi M, et al. Synaptotagmin VII splice variants alpha, beta, and delta are expressed in pancreatic beta-cells and regulate insulin exocytosis. FASEB J 2008;22:194–206
21. Gustavsson N, Lao Y, Maximov A, et al. Impaired insulin secretion and glucose intolerance in synaptotagmin-7 null mutant mice. Proc Natl Acad Sci USA 2008;105:3992–3997
22. Wu B, Wei S, Petersen N, et al. Synaptotagmin-7 phosphorylation mediates GLP-1-dependent potentiation of insulin secretion from β-cells. Proc Natl Acad Sci USA 2015;112:9996–10001
23. Andersson SA, Olsson AH, Esguerra JL, et al. Reduced insulin secretion correlates with decreased expression of exocytotic genes in pancreatic islets from patients with type 2 diabetes. Mol Cell Endocrinol 2012;364:36–45
24. Ostenson CG, Gaisano H, Sheu L, Tibell A, Bartfai T. Impaired gene and protein expression of exocytotic soluble N-ethylmaleimide attachment protein receptor complex proteins in pancreatic islets of type 2 diabetic patients. Diabetes 2006;55:435–440
25. Kwan EP, Gaisano HY. Glucagon-like peptide 1 regulates sequential and compound exocytosis in pancreatic islet beta-cells. Diabetes 2005;54:2734–2743
26. Liu Y, Batchuluun B, Ho L, et al. Characterization of zinc influx transporters (ZIPs) in pancreatic beta cells: roles in regulating cytosolic zinc homeostatsis and insulin secretion. J Biol Chem 2015;290:18757–18769
27. Xie L, Kang Y, Liang T, et al. RalA GTPase tethers insulin granules to L- and R-type calcium channels through binding α2 δ-1 subunit. Traffic 2013;14:428–439
28. Xie L, Zhu D, Kang Y, Liang T, He Y, Gaisano HY. Exocyst sec5 regulates exocytosis of newcomer insulin granules underlying biphasic insulin secretion. PLoS One 2013;8:e67561
29. Kasai K, Ohara-Imaizumi M, Takahashi N, et al. Rab27a mediates the tight docking of insulin granules onto the plasma membrane during glucose stimulation. J Clin Invest 2005;115:388–396
30. Xie L, Zhu D, Gaisano HY. Role of mammalian homologue of Caenorhabditis elegans unc-13-1 (Munc13-1) in the recruitment of newcomer insulin granules in both first and second phases of glucose-stimulated insulin secretion in mouse islets. Diabetologia 2012;55:2693–2702
31. Gustavsson N, Wei SH, Hoang DN, et al. Synaptotagmin-7 is a principal Ca2+ sensor for Ca2+-induced glucagon exocytosis in pancreas. J Physiol 2009;587:1169–1178
32. Maximov A, Lao Y, Li H, et al. Genetic analysis of synaptotagmin-7 function in synaptic vesicle exocytosis. Proc Natl Acad Sci USA 2008;105:3986–3991
33. Lovshin JA, Drucker DJ. Incretin-based therapies for type 2 diabetes mellitus. Nat Rev Endocrinol 2009;5:262–269
34. Braun M, Ramracheya R, Bengtsson M, et al. Voltage-gated ion channels in human pancreatic beta-cells: electrophysiological characterization and role in insulin secretion. Diabetes 2008;57:1618–1628
35. Bhalla A, Chicka MC, Chapman ER. Analysis of the synaptotagmin family during reconstituted membrane fusion. Uncovering a class of inhibitory isoforms. J Biol Chem 2008;283:21799–21807
36. Liu H, Bai H, Hui E, et al. Synaptotagmin 7 functions as a Ca2+-sensor for synaptic vesicle replenishment. eLife 2014;3:e01524
37. Südhof TC. Neurotransmitter release: the last millisecond in the life of a synaptic vesicle. Neuron 2013;80:675–690

38. Zhang Z, Hui E, Chapman ER, Jackson MB. Regulation of exocytosis and fusion pores by synaptotagmin-effector interactions. Mol Biol Cell 2010;21:2821–2831
39. Olofsson CS, Göpel SO, Barg S, et al. Fast insulin secretion reflects exocytosis of docked granules in mouse pancreatic B-cells. Pflugers Arch 2002;444:43–51
40. Lipstein N, Sakaba T, Cooper BH, et al. Dynamic control of synaptic vesicle replenishment and short-term plasticity by Ca(2+)-calmodulin-Munc13-1 signaling. Neuron 2013;79:82–96
41. Wiser O, Trus M, Hernández A, et al. The voltage sensitive Lc-type Ca2+ channel is functionally coupled to the exocytotic machinery. Proc Natl Acad Sci USA 1999;96:248–253
42. Jing X, Li DQ, Olofsson CS, et al. CaV2.3 calcium channels control second-phase insulin release. J Clin Invest 2005;115:146–154
43. Chicka MC, Hui E, Liu H, Chapman ER. Synaptotagmin arrests the SNARE complex before triggering fast, efficient membrane fusion in response to Ca2+. Nat Struct Mol Biol 2008;15:827–835
44. Bacaj T, Wu D, Yang X, et al. Synaptotagmin-1 and synaptotagmin-7 trigger synchronous and asynchronous phases of neurotransmitter release. Neuron 2013;80:947–959
45. Schonn JS, Maximov A, Lao Y, Südhof TC, Sørensen JB. Synaptotagmin-1 and -7 are functionally overlapping Ca2+ sensors for exocytosis in adrenal chromaffin cells. Proc Natl Acad Sci USA 2008;105:3998–4003
46. Gustavsson N, Wang X, Wang Y, et al. Neuronal calcium sensor synaptotagmin-9 is not involved in the regulation of glucose homeostasis or insulin secretion. PLoS One 2010;5:e15414